

# Particle-in-Cell modeling of a potential demonstration experiment for double pulse enhanced target normal sheath acceleration

Nashad Rahman,<sup>1, a)</sup> Joseph R. Smith,<sup>1, 2, 3</sup> Gregory Ngirmang,<sup>4, 5</sup> and Chris Orban<sup>1</sup>

<sup>1)</sup>Department of Physics, The Ohio State University, Columbus, OH, 43210, USA

<sup>2)</sup>Department of Materials Science and Engineering, The Ohio State University, Columbus, OH, 43210, USA

<sup>3)</sup>Air Force Institute of Technology, Dayton, OH, USA

<sup>4)</sup>National Academies of Sciences, Engineering, and Medicine, Washington DC, USA

<sup>5)</sup>Air Force Research Laboratory, Dayton, OH, USA

(Dated: 24 May 2022)

Ultra intense lasers are a promising source of energetic ions for various applications. An interesting approach described in Ferri et al. 2019 argues from Particle-in-Cell simulations that using two laser pulses of half energy (half intensity) arriving with close to 45 degrees angle of incidence is significantly more effective at accelerating ions than one pulse at full energy (full intensity). For a variety of reasons, at the time of this writing there has not yet been a true experimental confirmation of this enhancement. In this paper we perform 2D Particle-in-Cell simulations to examine if a millijoule class,  $5 \cdot 10^{18}$  Wcm<sup>-2</sup> peak intensity laser system could be used for such a demonstration experiment. Laser systems in this class can operate at a kHz rate which should be helpful for addressing some of the challenges of performing this experiment. Despite investigating a 3.5 times lower intensity than Ferri et al. 2019 did, we find that the double pulse approach enhances the peak proton energy and the energy conversion to protons by a factor of about three compared to a single laser pulse with the same total laser energy. We also comment on the nature of the enhancement and describe simulations that examine how the enhancement may depend on the spatial or temporal alignment of the two pulses.

## I. INTRODUCTION

Sources of energetic ions can be useful for a variety of industrial, biomedical, and defense applications<sup>1-7</sup>. However, the size and cost of conventional accelerators can limit the use of this technology. Ultra-intense laser systems can potentially serve as a compact source of energetic ions. As discussed, for example, in Palmer<sup>8</sup> laser technology is maturing rapidly towards this goal.

There are still a number of technical challenges involved in translating proof-of-concept laser experiments to real-world applications. Among these challenges, the need to maximize the number of energetic ions accelerated by the laser interactions and to increase the peak energy of these ions is paramount. Ferri, Siminos, and Fülöp<sup>9</sup>, Ferri *et al.*<sup>10</sup> outline an approach to increase the peak ion energy and numbers of energetic ions (without increasing the total laser energy) by dividing the laser energy into two laser pulses that irradiate the target from different angles. The authors refer to this approach as “enhanced Target Normal Sheath Acceleration” (enhanced TNSA). Ferri, Siminos, and Fülöp<sup>9</sup>, Ferri *et al.*<sup>10</sup> find best results for these two pulses arriving at 45 degree angles of incidence with pulses arriving at 40 degrees and 50 degrees performing almost as well. Recently, Jiang *et al.*<sup>11</sup> provided simulation results describing a similar approach to enhanced TNSA using three laser pulses instead of two. In the present work, we only discuss double pulse enhanced TNSA for simplicity and because a three pulse experiment is even more difficult to perform than a two pulse experiment.

From an experimental point of view, there are a number of challenges with implementing the double pulse setup. In order

for constructive interference to occur, both laser pulses need to arrive on target within the duration of the laser pulse. This can potentially be done using a delay line but it adds another element to the experiment that was not necessary for a single pulse. Once adequately synchronized, both micron scale laser spots need to spatially align despite instrumental vibrations. Perhaps because of these challenges, in their literature review Ferri, Siminos, and Fülöp<sup>9</sup> could only cite experimental papers where two pulses arrive on target from the same angle but with a time delay<sup>12-14</sup> and one paper in which an intense pulse reflects from the target and is redirected to the target area by reflecting from a spherical shell<sup>15</sup>. We note that<sup>16</sup> uses two pulses from different angles on two different targets in a multi stage approach to TNSA. However none of these experimental studies consider simultaneous double pulse irradiation of targets from two different angles of incidence like<sup>9,10</sup> propose. The closest experimental work that we could find is Morace *et al.*<sup>17</sup> who use the interference of four overlapping, picosecond timescale “beamlets” to create a periodic interference pattern that shapes the target during the interaction to enhance ion acceleration. These beamlets are aimed at the target with a relatively large spot size and small angles of incidence (a few degrees). That study finds enhanced ion acceleration but not nearly as much as<sup>9,10</sup> suggest is possible. Also, the mechanism that the authors propose is distinct from what<sup>9</sup> and<sup>10</sup> describe and requires a longer timescale.

An appealing platform for demonstrating double pulse enhanced TNSA that we consider in this paper would be a millijoule class short pulse laser system operating at a high repetition rate. Such an experiment would face a number of challenges. Instrumental vibrations will produce shot-to-shot variations in the position of the laser spots that could easily be larger than the width of the laser spot itself. An additional challenge would be ensuring that the laser pulses ar-

<sup>a)</sup>Electronic mail: rahman.176@osu.edu

rive within the duration of the pulse. But, if coupled to a data acquisition system capable of single shot analysis and a precision delay line, one could measure the ejected ion energy spectrum in rare events where both micron scale laser spots are well aligned spatially and temporally. Over time one can collect statistics that explore how the ejected proton spectrum depends on the distance between the spots and temporal alignment.

A particularly good example of a milliJoule class laser system with advanced diagnostics is the laser system used in Morrison *et al.*<sup>18</sup>. As described in Morrison *et al.*<sup>19</sup>, 5 mJ laser pulses with a peak intensity near  $5 \cdot 10^{18} \text{ W cm}^{-2}$  were used to accelerate protons up to 2.5 MeV in energy and at a kHz repetition rate. As discussed in a perspectives article by Palmer<sup>8</sup>, producing  $\sim 2$  MeV protons from a few mJ class laser system operating at a kHz repetition rate had not been achieved before.

In the present work we perform Particle-in-Cell (PIC) simulations in an effort to determine if the laser system described by Morrison *et al.*<sup>18</sup> could be a useful platform for demonstrating double pulse enhanced laser ion acceleration as described in Ferri, Siminos, and Fülöp<sup>9</sup>, Ferri *et al.*<sup>10</sup>. A key question is whether the  $5 \cdot 10^{18} \text{ W cm}^{-2}$  peak intensity laser pulses produced by this system, if split into two pulses and directed to the target, will produce enhanced ion acceleration even though the intensities involved are 3.5 times lower than the lowest intensity described in Ferri, Siminos, and Fülöp<sup>9</sup> and a different target is used. Given that the nature of the effect is not yet perfectly understood (as will be discussed later), and that there can be intensity thresholds in this range for various other kinds of laser phenomena (e.g.<sup>20,21</sup>), we can answer these questions with simulations rather than simply assuming that the double pulse approach will remain effective in the regime accessible through experiments with milliJoule class lasers. To provide additional guidance to our experimental colleagues, we also present additional simulation results that address how robust the enhanced proton energies are to spatial or temporal misalignment or phase offsets.

In Sec. II we describe our simulation setup. In Sec. III we describe our simulation results for perfect temporal and spatial alignment of the two pulses and compare to the single pulse case. In Sec. IV we present another set of simulation results that consider the impact of spatially or temporally misaligned pulses on the proton energies. In Sec. V we discuss the simulation results in both Sec. III and Sec. IV and comment on the nature of the effect. In Sec. VI we conclude.

## II. SIMULATION SETUP

We performed 2D3v PIC simulations using the LSP code<sup>22</sup> to simulate intense laser interactions with a  $0.46 \mu\text{m}$  thick Ethylene Glycol target. This target was irradiated with either a single beam with intensity of  $5 \cdot 10^{18} \text{ W cm}^{-2}$  or two beams of intensity  $2.5 \cdot 10^{18} \text{ W cm}^{-2}$ . All beams were  $780 \text{ nm}$  in wavelength and incident on the target p-polarized at  $45^\circ$  to normal and with a spot size of  $2.2 \mu\text{m}$  (FWHM) and a pulse width of  $42 \text{ fs}$  Full Width at Half Maximum (FWHM) with a

sine squared envelope. The single beam simulation (including laser and target) was overall similar to an experiment and simulation described in Morrison *et al.*<sup>18</sup> which demonstrated proton energies up to 2.5 MeV.

We used the implicit field advance and particle advance in the LSP code with 2D3v dimensionality. The simulation grid was 2800 by 2800 cells with a physical size of  $28 \mu\text{m} \times 28 \mu\text{m}$ . Each cell that contained target material used 9 particles each of protons, electrons, singly ionized Oxygen, and singly ionized Carbon resulting in 36 total particles per cell. The target electron density was  $10^{23} \text{ cm}^{-3}$  with other species in proportion to ensure that the target is neutral. Field ionization using the ADK model<sup>23</sup> was included in the simulations to allow Carbon and Oxygen ions to be further ionized by either the laser electric field or the electrostatic fields on the target<sup>23,24</sup>. No pre-plasma was assumed. Instead, there was only the maximum density or vacuum. The initial temperature of the particles was set at 1 eV. These simulations were run for 1 ps with 20 as timesteps.

In Sec. III we present simulations where the two laser pulses are perfectly aligned in terms of the laser spot and perfectly aligned temporally, meaning no time delay between the two pulses and the peak intensity reaches the target at the same time. In Sec. IV we present results from a number of simulations that consider misaligned pulses as described in that section. In both sections we compare to single pulse simulations with full intensity and energy and the same temporal duration.

## III. RESULTS FROM TEMPORALLY AND SPATIALLY WELL ALIGNED PULSES

Fig. 1 presents the electric fields normal to the target for the single pulse simulation (top panels) and the double pulse simulation (lower panels) at three different times. The first panel shows 50 fs after the beginning of the simulation when the pulses are beginning to interact with the target. The laser arriving from the top is polarized in the  $x$  direction and moving in the  $-z$  direction. The second laser pulse, which is polarized in the  $z$  direction, is moving in the  $+x$  direction towards the target. Because the target normal E fields are plotted in Fig. 1 it is easy to see both pulses in the bottom panel and only one pulse in the top panel.

The middle panels of Fig. 1 show the electric field component normal to the target at 100 fs after the start of the simulation. At this time, the laser pulse is strongly interacting and reflecting from the target, producing constructive and destructive interference. Only a small fraction of the pulse energy is transmitted through the target. Interestingly, the sheath fields at the back side of the target are highly symmetric in the double pulse simulation whereas the single pulse simulation is less symmetric and features a weaker electric field.

The right panels show at a time 150 fs after the start of the simulation, at which time the laser pulses have passed the target and are leaving the simulation. The sheath field in the double pulse simulation remains larger than the single pulse simulation and more symmetric. At the center of both of these panels, the target has visibly expanded due to the TNSA pro-

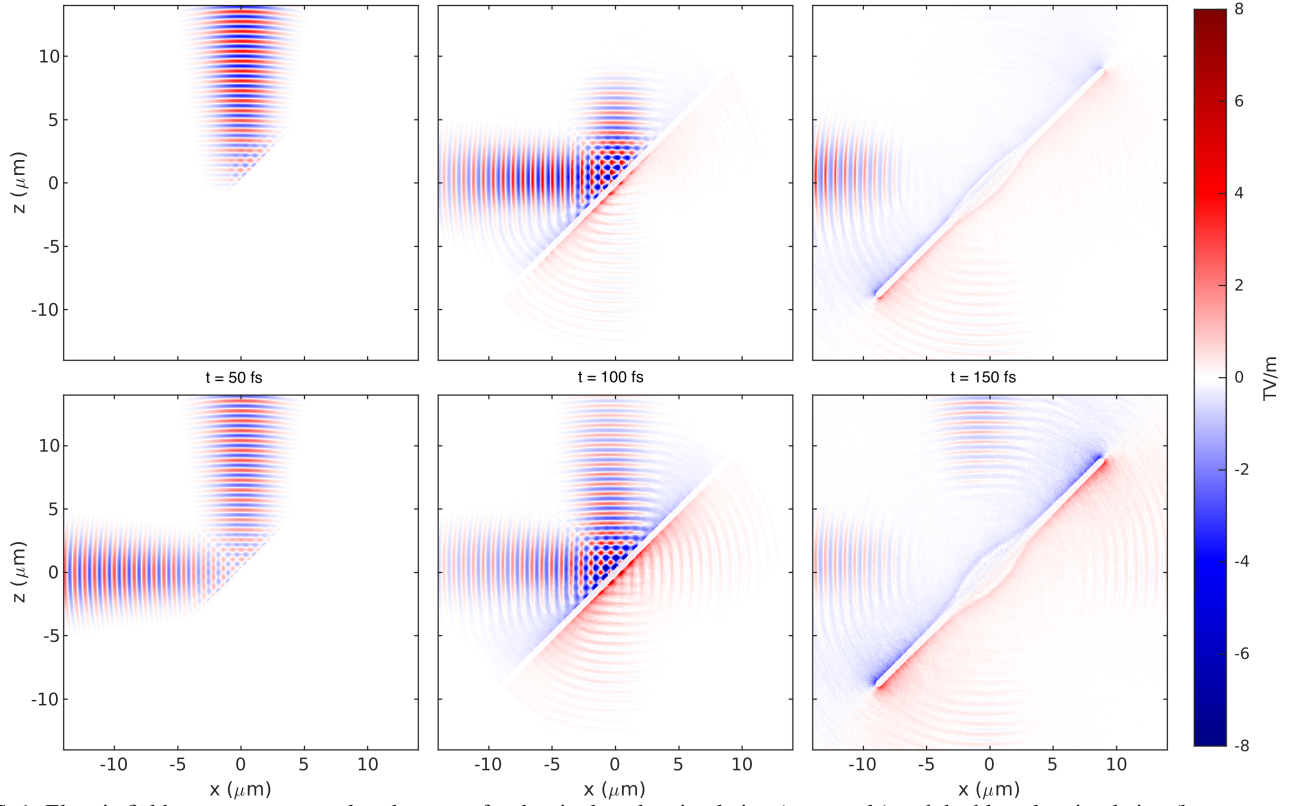


FIG. 1. Electric field component normal to the target for the single pulse simulation (top panels) and double pulse simulation (bottom panels) at 50 fs (left panels), 100 fs (center panels), and 150 fs (right panels)

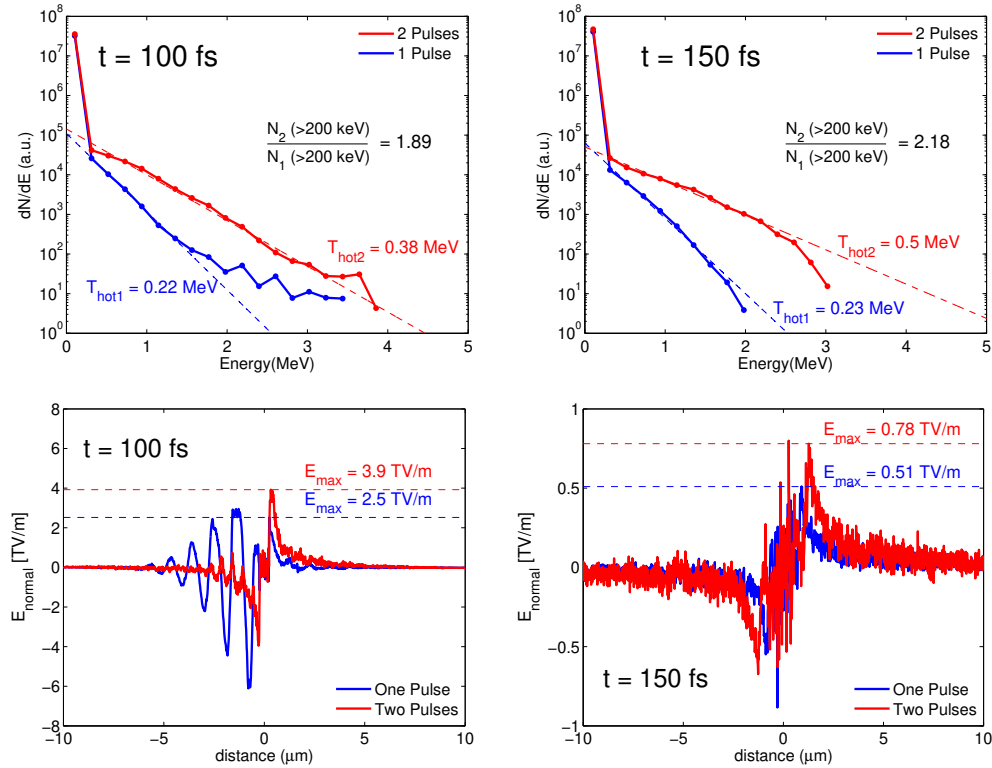


FIG. 2. Upper panels show electron energy spectra for 100 fs (left panel) and 150 fs (right panel) into the simulation. Lower panels show a lineup of the electric field perpendicular to the target with the left panel showing 100 fs and the right panel showing 150 fs. In the top panels the exponential fit (a.k.a. hot temperature) is shown with dashed lines and the ratio of electrons above 200 keV in energy is shown. In the bottom panels the maximum electric field on the side of the target away from the laser is highlighted with dashed horizontal lines.

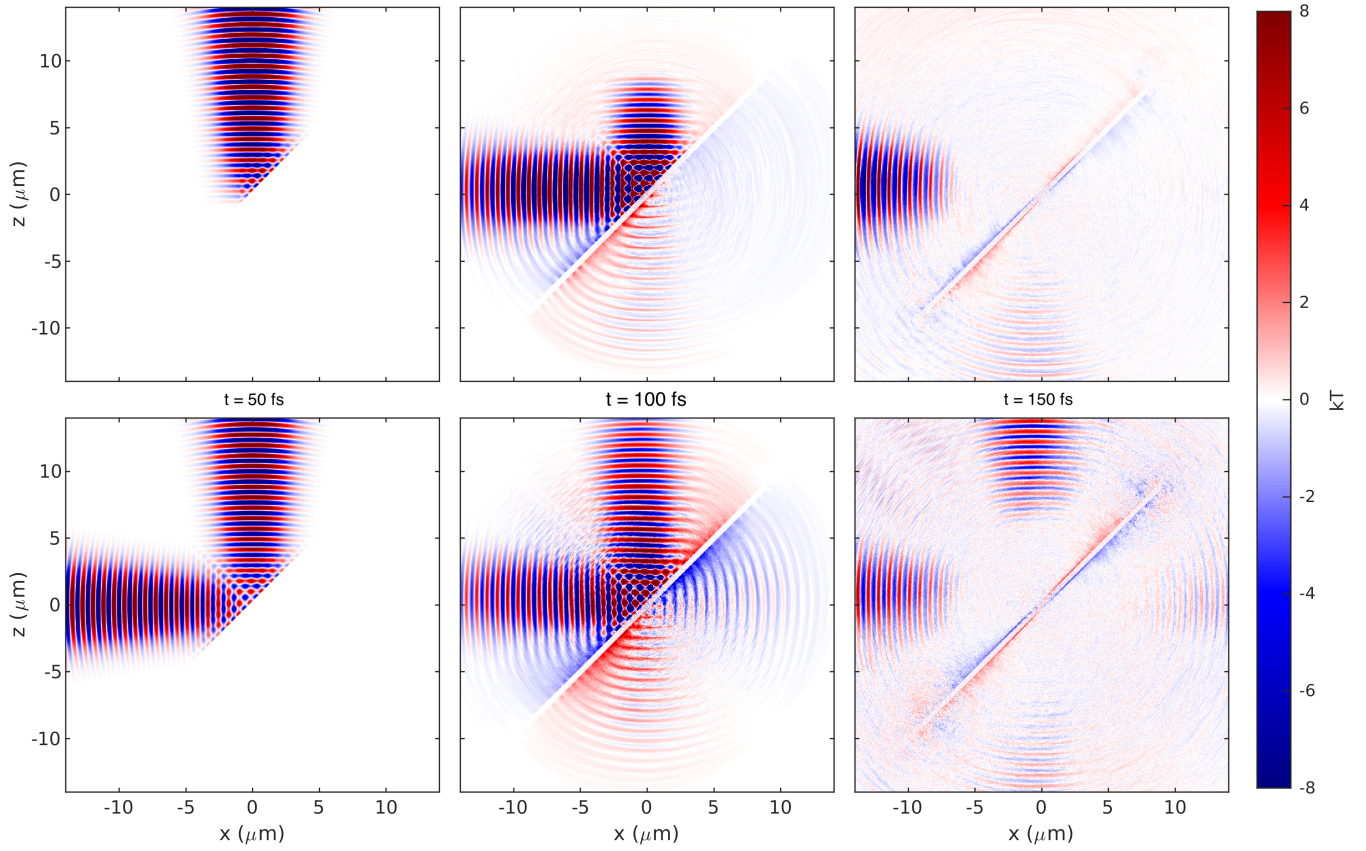


FIG. 3. Magnetic field component perpendicular to the plane of the simulation for the single pulse simulation (top panels) and double pulse simulation (bottom panels) at 50 fs (left panels), 100 fs (center panels), and 150 fs (right panels)

cess.

Figure 2 shows the electron energy spectra at 100 fs and 150 fs. At both times, electrons have a higher effective “hot” temperature and are more abundant for the double pulse case. For example, there are roughly twice as many electrons above 200 keV energy in the double pulse simulation. Figure 2 also includes lineouts of the electric field normal to the target showing noticeable enhancement of the accelerating field for the double pulse simulation by a factor of about 1.5.

Fig. 3 shows snapshots of the magnetic field at 50, 100 and 150 fs. Specifically we show the component of the magnetic field perpendicular to the plane of the simulation ( $B_y$ ).

Fig. 4 shows the positions and energies of a random selection of protons in our simulation 450 fs after the start of the simulation. The left panel is the single pulse simulation and the right panel is the double pulse simulation. We highlight 450 fs because the difference between the single pulse and double pulse simulations are particularly apparent at this time but it is still too early for protons to begin leaving the simulation. As the plot shows, the double pulse simulation has higher maximum proton energies than the single pulse simulation and these protons naturally travel further from the target by 450 fs.

The maximum proton energy in the simulation changes with time so it is important to illustrate this. The left panel

of Fig. 5 shows the average energy of the top 1000 proton macroparticles in the single and double pulse simulations. This figure shows a significantly sharper increase in the maximum proton energies of the double pulse simulation compared to the single pulse simulation. After 700 fs, the most energetic protons in the double pulse simulation begin to leave grid which is why the energies drop significantly. At 700 fs into the simulation, the average energy of the top 1,000 protons was 1.85 MeV for the single pulse simulation and 4.84 MeV for the double pulse simulation. This is a remarkable increase of 2.9 times greater proton energy, despite both simulations having the same total pulse energy.

The right panel of Fig. 5 shows the proton and ion spectra for both simulations at 700 fs. These spectra show an increase in the maximum proton energy from  $\sim 2$  MeV to  $\sim 5.5$  MeV as well as increases in the numbers of energetic protons and ions. Note that because the left panel of Fig. 5 is the average of the 1000 most energetic proton macroparticles that these average energies there are slightly lower than the peak energies seen in the energy spectra in the right panel of Fig. 5.

Fig. 6 compares the ejection angles and energies of the protons in both simulations at 450 fs calculated from the momenta of the proton macroparticles. Larger energy particles are further from the origin at the center of the plot. The TNSA process accelerates protons both in the forward direction from

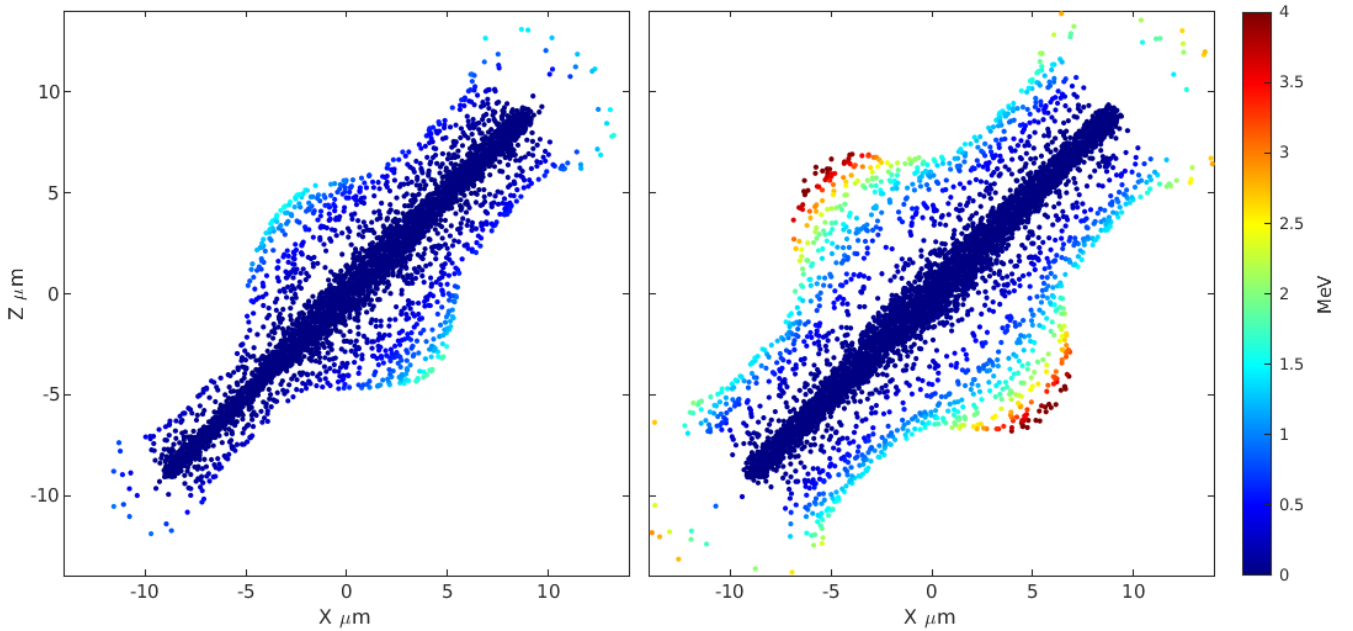


FIG. 4. (left panel) Proton energy 450 fs after pulse for single pulse. (right panel) Proton energy 450 fs after pulse for double pulse.

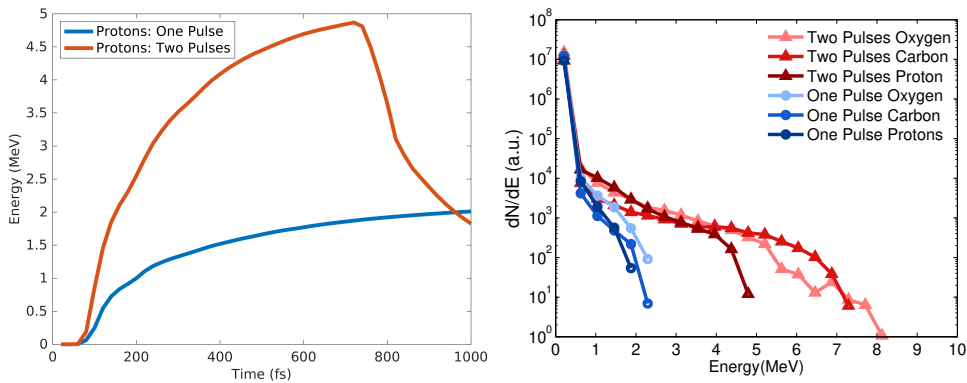


FIG. 5. (left panel) Average energy of the 1000 most energetic proton macroparticles in the single pulse and double pulse simulations. (right panel) Comparing ion spectra at 700 fs after the beginning of the simulation.

the target as well as the back (specular) direction. In Fig. 6, forward moving protons appear in the bottom right while back directed protons appear in the top left.

At 450 fs into the simulation, 79% of the protons above 300 keV in the single pulse simulation were found to have an ejection angle within  $\pm 5^\circ$  from normal to the target, compared to 69% for the double pulse simulation. Considering only the 1,000 proton macroparticles with the greatest energies at 450 fs, the percent of proton macroparticles which were found to have an ejection angle between within  $\pm 5^\circ$  from normal to the target was 86% in the single pulse simulation and 72% of the double pulse simulation. These 1000 most energetic proton macroparticles had an energy range between 1.41 MeV to 1.91 MeV in the single pulse simulation and from 3.83 MeV to 4.87 MeV in the double pulse simulation. Although the ions in the single pulse simulation are somewhat more collimated than the double pulse sim, it is important to note that there are significantly more protons with energies greater than 300 keV

in the double pulse simulation as discussed in the next section.

#### IV. RESULTS FROM TEMPORALLY OR SPATIALLY MISALIGNED PULSES

An important question for experimental demonstration is how closely the two beams must overlap, both spatially and temporally, to see a significant increase in peak ion energy and whether the phases of the two beams matter. In experiment, aligning two beams with high precision can be challenging and the beams may shift slightly between shots. These shot-to-shot variations (sometimes called jitter) can cause inconsistently aligned pulses. With this in mind we performed a number of additional 2D3v PIC simulations using the same setup described in Sec II but with spatial, temporal or phase offsets.

Fig. 7 shows the maximum proton energy from additional

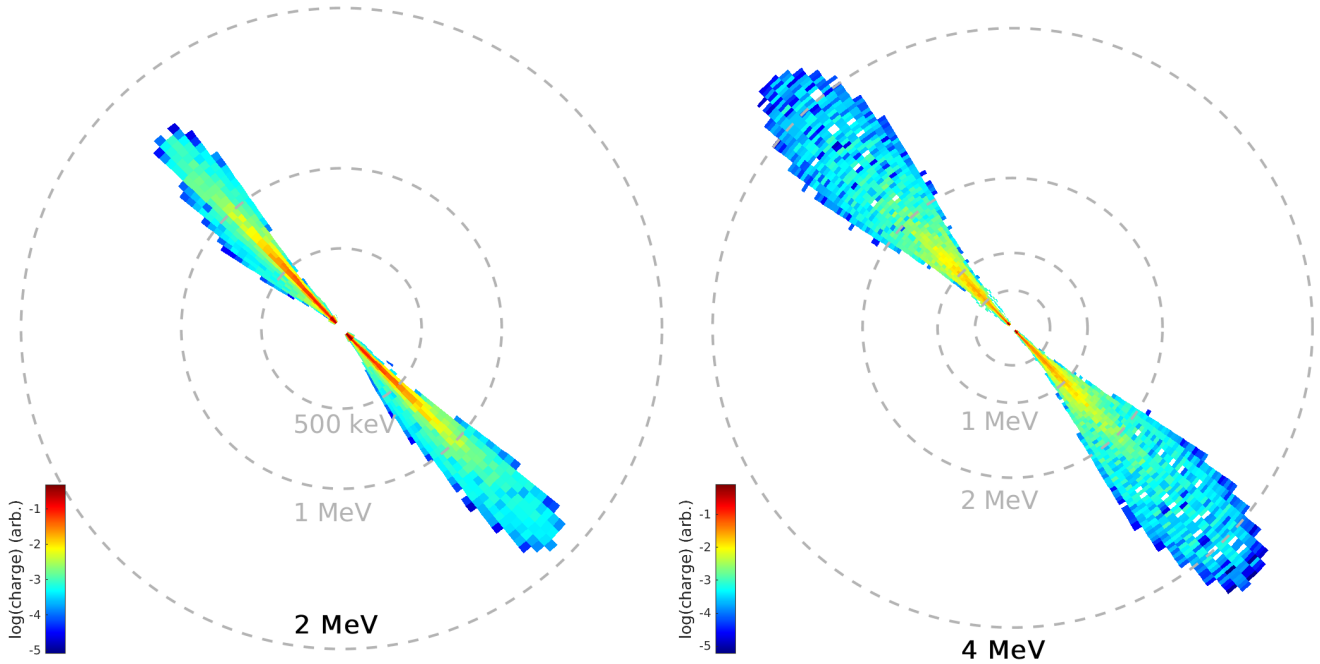


FIG. 6. An analysis of the ejection angles and energies of protons in the single pulse (left panel) and double pulse (right panel) simulations at 450 fs. The protons are binned both by ejection angle and energy with the color proportional to the log of the number of proton macroparticles in that bin. Forward going protons appear in the bottom right of the plot while back-directed protons appear in the top left. Note that the scales for the energy are different across the two figures.

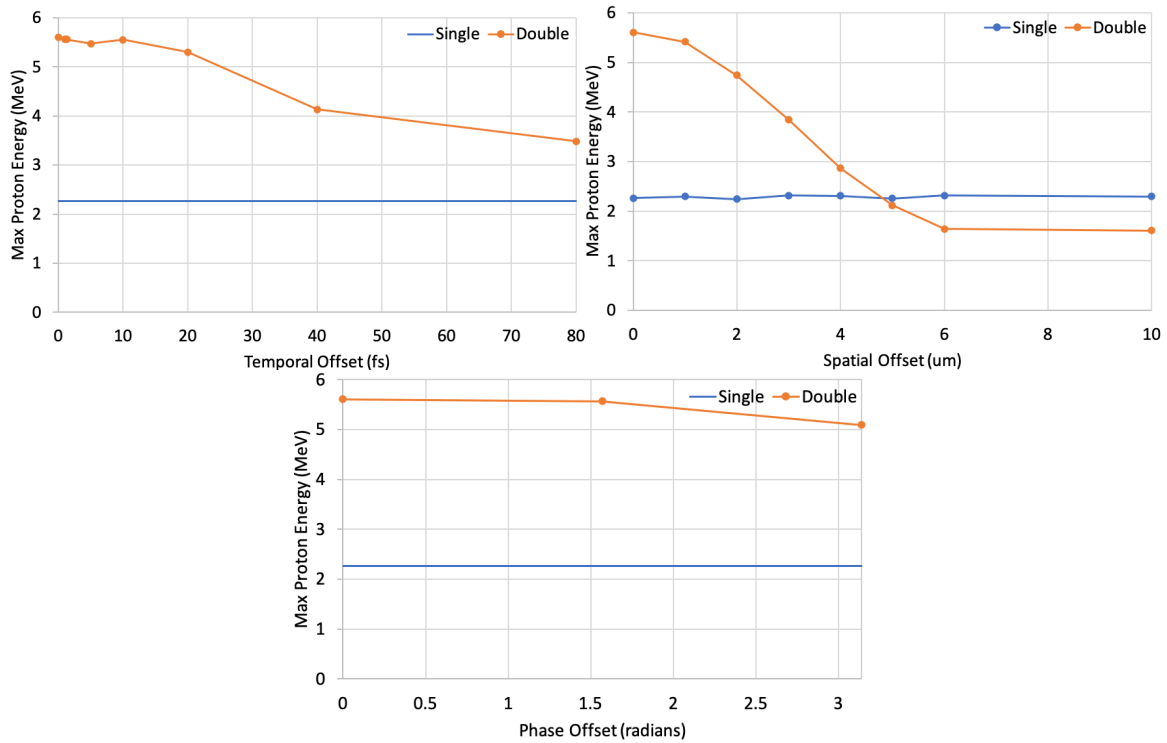


FIG. 7. Maximum proton energy at 750 fs after the start of the simulation for various temporal offsets (top left), spatial offsets (top right), and phase offsets (bottom). The top left panel shows temporal offsets ranging from 1 fs to 80 fs. The double pulse simulations had one pulse delayed and the other pulse with no delay. The maximum proton energy for the single pulse simulation is shown with a horizontal line. The top right panel shows spatial offsets ranging from 1  $\mu\text{m}$  to 10  $\mu\text{m}$ . The bottom panel shows phase offsets ranging from 0 to  $\pi$  radians.

2D3v PIC simulations using the same setup described in Sec II but with spatial, temporal or phase offsets. The top left panel of Fig. 7 shows the effect of temporal offsets and the top right panel of Fig. 7 shows the effect of spatial offsets on the maximum proton energies at 750 fs after the start of the simulation. By temporal offset we mean that one of the beams had a time delay. By spatial offsets we mean that both beams were moved evenly away from the center of the target without changing the angle of incidence. Both the single and double pulse beam positions were further adjusted to ensure that the peak focus (i.e. maximum intensity) remained at the target despite this change. The distance between the peak focus of the two beams is represented in the figure (i.e. the distance from the center of the target to the peak focus is half the distance represented in the figure). Both upper panels show a decrease in peak ion energy as the two beams are further from perfect temporal and spatial alignment. We also performed two additional simulations with perfect temporal and spatial overlap where the phase was offset in one of the beams.

Fig. 7 shows that the double pulse scheme still produces approximately a factor of two enhancement in max proton energy even for pulses that are 40 fs delayed or that are spatially offset by about 3  $\mu\text{m}$ . We did not perform simulations with both a spatial and temporal offset even though real experiments will likely have some degree of misalignment in both respects. The two simulations we performed to examine phase offsets found that the maximum proton energy only decreased (at most) by 10%.

## V. ANALYSIS AND DISCUSSION

The stated aim of this paper is to simulate a potential demonstration experiment of “enhanced TNSA” which is a phenomenon described by Ferri, Siminos, and Fülöp<sup>9</sup> and Ferri *et al.*<sup>10</sup>. In this section we comment on the nature of the enhancement as seen in our simulations which we include as an important background for what a potential demonstration experiment should try to measure. We also summarize some of the comments on the nature of the enhancement mentioned in<sup>9,10</sup>. Additional considerations for the required spatial and temporal alignment of the two pulses and robustness to phase differences are also discussed.

We compared the evolution of the energies in the two simulations from Sec. III in Fig. 8. We created this plot from the reported total energy in particles of various species versus time in the simulation, from measurements of the total “field energy” which is the sum of energy in electric fields and magnetic fields everywhere in the simulation versus time and from measurements of the electromagnetic energy leaving the grid. Our simulations also include an approximate estimate for energy loss due to purely numerical effects like the damping of the electromagnetic fields from the implicitness used by the LSP code. The sum of all these energy components add up to nearly the total energy of the laser energy entering the simulation (horizontal dashed line). Deviation from 100% is likely due to the approximate nature of the model that determines the estimated energy loss due to numerical effects. The estimated

numerical energy loss were similar with reported 5.43% energy loss for the single pulse simulation and 8.15% for the double pulse simulation after 1 picosecond of simulated time.

The difference between the left and right panels of Fig. 8 is striking. According to these data, 21% of the laser light is absorbed in the single pulse simulation while 53% of the light is absorbed in the double pulse case. This increased absorption ultimately produces 2.25 times more energy in electrons. So we conclude that a demonstration experiment should see a significant increase in absorption and corresponding decrease in reflected laser light.

Fig. 2, which shows the electron energy distributions in the upper panels, is insightful for understanding the difference in total electron energy in the two simulations. Both the numbers of energetic electrons and the energies of electrons are enhanced. According to Ferri, Siminos, and Fülöp<sup>9</sup> the reason for the enhanced electron acceleration (which of course is related the increased absorption) is due to better constructive interference of the laser electric fields on the target. As they illustrate, in the double pulse case the two beams constructively interfere even before reaching the target while the single pulse case can only interfere with its reflection (which is attenuated due to the absorption). Ultimately the strongest constructive interference occurs for the double pulse case. According to Eq. 1 in<sup>9</sup>, the constructive interference should enhance the electric field by a factor of  $\sqrt{2}$ , ultimately doubling the effective laser intensity near the target. We can examine whether the measured hot temperatures ( $T_{\text{hot}}$ ) from our simulations are consistent with this result. Using ponderomotive arguments for  $T_{\text{hot}}$  (e.g. Eq. 6 from<sup>25</sup>) with  $a_0 = 1.5$  for the single pulse simulation, the expected hot temperature for electrons is 0.23 MeV. Twice this intensity would imply  $a_0 = 2.1$  and the same formula would predict a hot temperature of 0.41 MeV. These numbers are very similar to the values we obtain in the upper panels of Fig. 2. Other scaling formulae (cf.<sup>26</sup> and references therein) give qualitatively similar results.

Another interesting consistency check that can be done with Fig. 2 is to see if the enhanced electric field that develops on the target is consistent with expectations from TNSA theory. As is well known (e.g.<sup>27,28</sup>), according to 1D arguments, the maximum electric field  $E_{\text{max}}$  should scale as  $k_B T_{\text{hot}}/e\lambda_D$  where  $\lambda_D$  is the Debye length and the Debye length should scale as  $\sqrt{k_B T_{\text{hot}}/n_{\text{hot}}}$  where  $n_{\text{hot}}$  is the density of hot electrons. This predicts a scaling of  $E_{\text{max}} \sim \sqrt{n_{\text{hot}} k_B T_{\text{hot}}}$ . Fig. 2 includes a measurement of the ratio of the hot electron density for electrons above an energy threshold of 200 keV. (The energy threshold of 200 keV is similar to the ponderomotive energy.) Broadly we find that hot electron density and the hot electron temperature are both enhanced by a factor of two which predicts an increased  $E_{\text{max}}$  by a factor of  $\approx \sqrt{2} \cdot 2 = 2$ . The enhancement in  $E_{\text{max}}$  from the bottom panels of Fig. 2 is measured to be close to 1.5. We note that using a 50% lower electron energy threshold reduces the enhancement in  $n_{\text{hot}}$  without significantly changing  $T_{\text{hot}}$ , bringing the predicted and measured enhancement in  $E_{\text{max}}$  into reasonable agreement. We regard these results as qualitative evidence that TNSA is the dominant ion acceleration mechanism in both simulations.

There is an interesting discussion in Ferri *et al.*<sup>10</sup> that proposes that differences in the structure of the quasi-static magnetic fields that develop on the target is another important reason why ion acceleration is more efficient for the double pulse case. In future work we intend to consider this question in depth with particle tracking. For the present work, it bears mentioning that the magnetic fields that develop on the target in our simulations (Fig. 3) have a structure that greatly resembles magnetic fields shown in Ferri *et al.*<sup>10</sup> which were obtained from higher intensity simulations. This raises our confidence that double pulse experiments at  $\sim 5 \cdot 10^{18} \text{ W cm}^{-2}$  intensities on millijoule class laser systems can provide useful insights to anticipate how experiments at much higher intensities would perform.

In terms of the still-unverified hypothesis that quasi-static magnetic fields play an important role in producing the enhancement we offer one insight: our double pulse simulations are more effective at converting electron energy to ion energy than the single pulse simulations. Because the ion acceleration happens on a similar or longer timescale that quasi-static magnetic fields develop it is plausible that magnetic fields are key to this result. In the single pulse simulations we found that 28% of the electron energy is ultimately converted to proton energy with another 26% going to Oxygen and Carbon. In the double pulse simulations 43% of the electron energy is converted to proton energy and 32% of the electron energy is converted to Oxygen and Carbon ions. So not only is there more energy in electrons in the double pulse simulations (as mentioned earlier), a higher fraction of this electron energy serves to accelerate ions. Ultimately the 2.25x increased energy in electrons combined with the enhanced transfer of that energy to ions produces a factor of 3.4 times as much energy in protons and a factor of 2.8 times as much energy in Oxygen and Carbon in the double pulse simulations. As mentioned earlier, the maximum energies of the ions are also significantly increased by a factor of 2.5-3 (Fig. 5). Interestingly, this is an even larger enhancement than was seen in<sup>9,10</sup>. A possible explanation for this could be that Ferri, Siminos, and Fülöp<sup>9</sup>, Ferri *et al.*<sup>10</sup> both simulate already fully ionized targets whereas our simulations include a prescription for ionizing ion species through field ionization as discussed in Sec. II. We performed simulations with fixed ionization (not shown), keeping all species singly ionized, and found that the enhancement in the numbers of protons and peak proton energy in the double pulse simulation compared to the single pulse simulation was less than what we found in Figs. 5 for the ionization simulations and closer to the factor of two that Ferri, Siminos, and Fülöp<sup>9</sup>, Ferri *et al.*<sup>10</sup> found.

In an effort to provide useful information to experimentalists regarding the possibility that the two pulses may be temporally or spatially misaligned we performed a number of additional simulations as presented in Sec. IV and highlighted in Fig. 7. Those simulations found that ion acceleration remained enhanced (compared to a single pulse simulation) by roughly factor of two even for temporal offsets of 40 fs. Given that the nature of the effect requires the constructive interference of the two pulses it is unsurprising that the effect is diminished when the delay becomes comparable to the 42 fs

FWHM duration of the pulses. At 80 fs, a smaller enhancement still remains. In Sec. I we mentioned studies where enhanced ion acceleration is found from two pulses arriving on target from the same angle but with a time delay<sup>12-14,29</sup>. Enhancement can potentially occur if the first pulse creates a pre-plasma on the target that increases the coupling of energy from the second pulse. A similar physical mechanism is explored, at higher intensities, in<sup>30</sup>.

Another set of simulations presented in Sec. IV found that pulses that were temporally aligned (zero delay) but with a spatial offset between  $2 \mu\text{m}$  and  $3 \mu\text{m}$  still enhanced the ion energies by about a factor of two compared to a single pulse simulation. In our simulations the spot sizes were both  $2.2 \mu\text{m}$  FWHM. Our results confirm intuition that aligning the laser spots within the FWHM of the spot size is important for producing the enhancement.

For brevity we did not perform simulations with both a spatial and temporal offset even though spatial and temporal offsets are likely on some level in any real demonstration experiment. Sec. IV does present simulations with different phase offsets between the two pulses, finding that, for our parameters, the maximum proton energy is robust to phase differences.

Other important questions remain including whether the enhancement of ion acceleration at the levels we have found persist when these simulations are performed in 3D instead of 2D3v geometry. Ferri, Siminos, and Fülöp<sup>9</sup> perform 3D simulations and found reasonable agreement with the 2D3v results. There are also a number of questions about the role of the quasi-static magnetic fields that particle tracking would illuminate. We have begun this analysis (not shown) but find that the substantial difference in absorption in the two simulations makes it difficult to pinpoint the role of the magnetic field separately from the role of the increased absorption. Another interesting investigation would be to consider three laser pulses (for the same total energy) as proposed recently by Jiang *et al.*<sup>11</sup>. We defer these questions for future work.

## VI. CONCLUSION

Using 2D3v PIC simulations we consider if a scenario for double pulse enhanced TNSA, as described by Ferri, Siminos, and Fülöp<sup>9</sup> and Ferri *et al.*<sup>10</sup>, would be feasible on a millijoule class laser system. For a number of practical reasons, at the time of this writing their idea of enhancing ion acceleration using two laser pulses with half energy (and intensity) and a wide ( $\sim 45^\circ$  angle of incidence) has not yet been convincingly demonstrated experimentally even though simulations predict substantially enhanced ion acceleration. We performed simulations with laser pulses that were 3.5 times less intense than the lowest intensity investigated in Ferri, Siminos, and Fülöp<sup>9</sup> and we used a different target material and target thickness than was used there. We assumed laser parameters similar to the millijoule class laser system described in Morrison *et al.*<sup>18</sup> which previously demonstrated up to 2.5 MeV protons. Comparing two pulses with intensities of  $2.5 \cdot 10^{18} \text{ W cm}^{-2}$  on target to a single  $5 \cdot 10^{18} \text{ W cm}^{-2}$  pulse

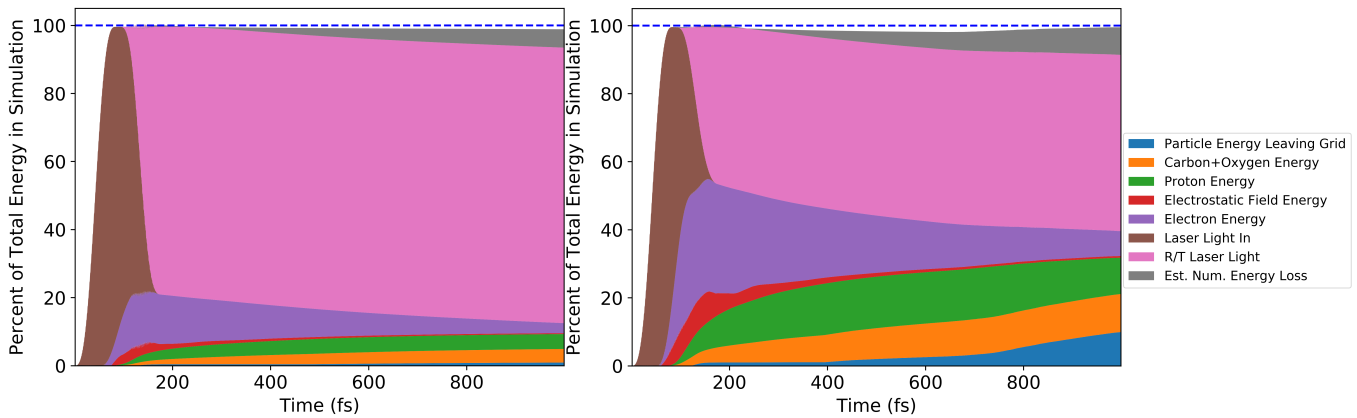


FIG. 8. Evolution of various sources of energy in the Single Pulse (left panel) and Double Pulse (right panel) simulations. A horizontal dashed line shows the analytically derived total laser energy that enters the simulation. The LSP code includes an approximate estimate of energy loss due to numerical effects which is shown on the plot. Also included is an estimate of the laser energy that leaves the simulation through reflection or transmission. The lines do not all add up to 100% likely due to the approximate nature of the estimate for energy loss due to numerical effects in the LSP code.

with the same pulse duration and spot size, our simulations find enhanced peak proton energy and conversion efficiency from laser energy to proton and ion energy by about a factor of 3 and with a similar divergence for protons. Interestingly, this factor of 3 enhancement is larger than the overall factor of 2 enhancement described in Ferri, Siminos, and Fülöp<sup>9</sup>.

We also find that the results for the electric and magnetic fields in our simulations qualitatively resemble snapshots of the electric and magnetic fields presented in Ferri, Siminos, and Fülöp<sup>9</sup> and Ferri *et al.*<sup>10</sup> from simulations performed at higher intensities. This implies that the constructive interference and quasi-static magnetic field generation occurs analogously at our lower intensity. We also present results from a series of simulations that examine the spatial or temporal misalignment of the two laser pulses or phase differences.

Investigation into the nature of the enhancement seems to confirm that TNSA is the dominant acceleration mechanism and that constructive interference provides a reasonable explanation for the enhancement in the electron energy distribution.

Our results lead us to the conclusion that millijoule class laser systems can play an important role in demonstrating double pulse enhanced TNSA. Such an experiment should be insightful for later experiments at much higher intensities and energies.

## ACKNOWLEDGMENTS

This research was supported in part by an appointment to the Postgraduate Research Participation Program at the U.S. Air Force Institute of Technology, administered by the Oak Ridge Institute for Science and Education through an interagency agreement between the U.S. Department of Energy and AFIT. This research is also supported by the Air Force Office of Scientific Research under LRIR Project 17RQCOR504 under the management of Dr. Andrew Stickrath. NR acknowledges summer support from the OSU SCARLET laser group. Simulations were performed on the ASC Unity cluster at Ohio

State University and the Ohio Supercomputer Center<sup>31</sup>.

## DATA AVAILABILITY

The data that support the findings of this study are available from the corresponding author upon reasonable request.

- <sup>1</sup>S. V. Bulanov and V. S. Khoroshkov, “Feasibility of using laser ion accelerators in proton therapy,” *Plasma Physics Reports* **28**, 453–456 (2002).
- <sup>2</sup>Y. I. Salamin, Z. Harman, and C. H. Keitel, “Direct high-power laser acceleration of ions for medical applications,” *Phys. Rev. Lett.* **100**, 155004 (2008).
- <sup>3</sup>A. Haque and S. Sumaiya, “An overview on the formation and processing of nitrogen-vacancy photonic centers in diamond by ion implantation,” *Journal of Manufacturing and Materials Processing* **1** (2017), 10.3390/jmmp1010006.
- <sup>4</sup>X. Tian, K. Liu, Y. Hou, J. Cheng, and J. Zhang, “The evolution of proton beam therapy: Current and future status,” *Molecular and clinical oncology* **8**, 15–21 (2018).
- <sup>5</sup>A. Ene, I. V. Popescu, and C. Stihl, “Applications of proton-induced x-ray emission technique in materials and environmental science,” *Ovidius Univ Ann Chem* **20**, 35–39 (2009).
- <sup>6</sup>I. Jain and G. Agarwal, “Ion beam induced surface and interface engineering,” *Surface Science Reports* **66**, 77–172 (2011).
- <sup>7</sup>K. E. Kippen, R. D. Fulton, E. Brown, W. T. Buttler, A. J. Clarke, K. K. Kwiatkowski, F. G. Mariani, F. E. Merrill, C. Morris, R. T. Olson, and M. Zellner, “Aot & lansce focus: Proton radiography facility,” [https://lansce.lanl.gov/facilities/pRad/\\_assets/docs/AOT-LANSCE-Pulse-pRad.pdf](https://lansce.lanl.gov/facilities/pRad/_assets/docs/AOT-LANSCE-Pulse-pRad.pdf) (2013).
- <sup>8</sup>C. Palmer, “Paving the way for a revolution in high repetition rate laser-driven ion acceleration,” *New Journal of Physics* **20**, 061001 (2018).
- <sup>9</sup>J. Ferri, E. Siminos, and T. Fülöp, “Enhanced target normal sheath acceleration using colliding laser pulses,” *Communications Physics* **2**, 40 (2019).
- <sup>10</sup>J. Ferri, E. Siminos, L. Gremillet, and T. Fülöp, “Effects of oblique incidence and colliding pulses on laser-driven proton acceleration from relativistically transparent ultrathin targets,” *Journal of Plasma Physics* **86**, 905860505 (2020).
- <sup>11</sup>X. Jiang, F. Shao, D. Zou, M. Yu, L. Hu, X. Guo, T. Huang, H. Zhang, S. Wu, G. Zhang, T. Yu, Y. Yin, H. Zhuo, and C. Zhou, “Energetic deuterium-ion beams and neutron source driven by multiple-laser interaction with pitcher-catcher target,” *Nuclear Fusion* **60**, 076019 (2020).
- <sup>12</sup>K. Markey, P. McKenna, C. M. Brenner, D. C. Carroll, M. M. Günther, K. Harres, S. Kar, K. Lancaster, F. Nürnberg, M. N. Quinn, A. P. L. Robinson, M. Roth, M. Zepf, and D. Neely, “Spectral enhancement in the double

- pulse regime of laser proton acceleration,” *Phys. Rev. Lett.* **105**, 195008 (2010).
- <sup>13</sup>C. M. Brenner, A. P. L. Robinson, K. Markey, R. H. H. Scott, R. J. Gray, M. Rosinski, O. Deppert, J. Badziak, D. Batani, J. R. Davies, S. M. Hassan, K. L. Lancaster, K. Li, I. O. Musgrave, P. A. Norreys, J. Pasley, M. Roth, H.-P. Schlenvoigt, C. Spindloe, M. Tatarakis, T. Winstone, J. Wolowski, D. Wyatt, P. McKenna, and D. Neely, “High energy conversion efficiency in laser-proton acceleration by controlling laser-energy deposition onto thin foil targets,” *Applied Physics Letters* **104**, 081123 (2014), <https://doi.org/10.1063/1.4865812>.
- <sup>14</sup>J. Ferri, L. Senje, M. Dalui, K. Svensson, B. Aurand, M. Hansson, A. Persson, O. Lundh, C.-G. Wahlström, L. Gremillet, E. Siminos, T. C. DuBois, L. Yi, J. L. Martins, and T. Fülöp, “Proton acceleration by a pair of successive ultraintense femtosecond laser pulses,” *Physics of Plasmas* **25**, 043115 (2018), <https://doi.org/10.1063/1.5026391>.
- <sup>15</sup>G. G. Scott, J. S. Green, V. Bagnoud, C. Brabetz, C. M. Brenner, D. C. Carroll, D. A. MacLellan, A. P. L. Robinson, M. Roth, C. Spindloe, F. Wagner, B. Zielbauer, P. McKenna, and D. Neely, “Multi-pulse enhanced laser ion acceleration using plasma half cavity targets,” *Applied Physics Letters* **101**, 024101 (2012), <https://doi.org/10.1063/1.4734397>.
- <sup>16</sup>W. P. Wang, B. F. Shen, H. Zhang, X. M. Lu, J. F. Li, S. H. Zhai, S. S. Li, X. L. Wang, R. J. Xu, C. Wang, Y. X. Leng, X. Y. Liang, R. X. Li, and Z. Z. Xu, “Multi-stage proton acceleration controlled by double beam image technique,” *Physics of Plasmas* **25**, 063116 (2018), <https://doi.org/10.1063/1.5022347>.
- <sup>17</sup>A. Morace, N. Iwata, Y. Sentoku, K. Mima, Y. Arikawa, A. Yogo, A. Andreev, S. Tosaki, X. Vaisseau, Y. Abe, S. Kojima, S. Sakata, M. Hata, S. Lee, K. Matsuo, N. Kamitsukasa, T. Norimatsu, J. Kawanaka, S. Tokita, N. Miyanaga, H. Shiraga, Y. Sakawa, M. Nakai, H. Nishimura, H. Azechi, S. Fujioka, and R. Kodama, “Enhancing laser beam performance by interfering intense laser beamlets,” *Nature Communications* **10**, 2995 (2019).
- <sup>18</sup>J. T. Morrison, S. Feister, K. D. Frische, D. R. Austin, G. K. Ngirmang, N. R. Murphy, C. Orban, E. A. Chowdhury, and W. M. Roquemore, “MeV proton acceleration at kHz repetition rate from ultra-intense laser liquid interaction,” *New Journal of Physics* **20**, 022001 (2018).
- <sup>19</sup>J. T. Morrison, E. A. Chowdhury, K. D. Frische, S. Feister, V. M. Ovchinnikov, J. A. Nees, C. Orban, R. R. Freeman, and W. M. Roquemore, “Backward-propagating MeV electrons from  $10^{18}$  W/cm<sup>2</sup> laser interactions with water,” *Physics of Plasmas* **22**, 043101 (2015), arXiv:1501.02261 [physics.plasm-ph].
- <sup>20</sup>C. Orban, J. T. Morrison, E. D. Chowdhury, J. A. Nees, K. Frische, and W. M. Roquemore, “Backward-Propagating MeV Electrons in Ultra-Intense Laser Interactions: Standing Wave Acceleration and Coupling to the Reflected Laser Pulse,” *Physics of Plasmas* (2015).
- <sup>21</sup>J. R. Smith, C. Orban, G. K. Ngirmang, J. T. Morrison, K. M. George, E. A. Chowdhury, and W. M. Roquemore, “Particle-in-cell simulations of density peak formation and ion heating from short pulse laser-driven ponderomotive steepening,” *Physics of Plasmas* **26**, 123103 (2019), <https://doi.org/10.1063/1.5108811>.
- <sup>22</sup>D. R. Welch, D. V. Rose, R. E. Clark, T. C. Genoni, and T. P. Hughes, “Implementation of a non-iterative implicit electromagnetic field solver for dense plasma simulation,” *Computer Physics Communications* **164**, 183–188 (2004).
- <sup>23</sup>M. V. Ammosov, N. B. Delone, and V. P. Krainov, “Tunnel ionization of complex atoms and of atomic ions in an alternating electromagnetic field,” *Sov. Phys. JETP* **64**, 1191–1194 (1986).
- <sup>24</sup>A. M. Perelomov, V. S. Popov, and M. V. Terent’ev, “Ionization of atoms in an alternating electrical field,” *Sov. Phys. JETP* **23**, 924 (1966).
- <sup>25</sup>A. Macchi, M. Borghesi, and M. Passoni, “Ion acceleration by superintense laser-plasma interaction,” *Rev. Mod. Phys.* **85**, 751–793 (2013).
- <sup>26</sup>M. G. Haines, M. S. Wei, F. N. Beg, and R. B. Stephens, “Hot-electron temperature and laser-light absorption in fast ignition,” *Phys. Rev. Lett.* **102**, 045008 (2009).
- <sup>27</sup>P. Mora, “Plasma expansion into a vacuum,” *Phys. Rev. Lett.* **90**, 185002 (2003).
- <sup>28</sup>M. Roth and M. Schollmeier, “Ion acceleration – target normal sheath acceleration,” in *Proceedings of the 2014 CAS-CERN Accelerator School* (2016).
- <sup>29</sup>S. Kumar and D. N. Gupta, “Optimization of laser parameters for proton acceleration using double laser pulses in tnsa mechanism,” *Laser and Particle Beams* **38**, 73–78 (2020).
- <sup>30</sup>J. Kim, D. Mariscal, S. Wilks, A. Kemp, T. Ma, and F. Beg, “Continuous Laser-Driven Ion Acceleration through Two-Stage Boosting,” in *APS Division of Plasma Physics Meeting Abstracts*, APS Meeting Abstracts, Vol. 2020 (2020) p. PO03.010.
- <sup>31</sup>OSC, “Ohio supercomputer center,” <http://osc.edu/ark:/19495/f5s1ph73> (1987).